Correlation of Icing Relationships with Airfoil and Rotorcraft Icing Data

Robert J. Flemming* and David A. Lednicer†
United Technologies Corporation, Stratford, Connecticut

A high-speed icing wind tunnel test program was conducted to measure the ice growth and performance degradation on 10 rotorcraft airfoil models for ranges of liquid-water content, temperature, and Mach number at several steady and unsteady angles of attack. Prior to these tests, airfoil icing data had been acquired only in low-speed tunnels or during flight testing, but high-speed data are necessary for the prediction of icing on rotors. The test explored the boundaries for the onset of icing and between glaze and rime ice. Ice shapes were documented and lift, drag, and pitching moment were measured. Airfoil lift was reduced slightly at low angles of attack and about 20% at high angles. Drag increased in moderate icing at low angles of attack by a factor of three to four, increasing for higher liquid-water contents and angles above 6 deg. The effect of Mach number varied. Airfoil oscillation did not change the lift loss, but did reduce the drag penalty. Two-dimensional airfoil icing relationships for ice thickness and for changes in lift, drag, and pitching moment coefficients were formulated, with improved accuracy over prior relationships. These relationships have been used to predict aircraft power changes during icing.

Nomenclature

c	= airfoil chord, m
C_d	= drag coefficient
C_ℓ	= lift coefficient
C_m	= pitching moment coefficient
D_d	= droplet diameter, μm
E	= total airfoil collection efficiency
k/c	= roughness height-to-chord ratio
k_0	= modified inertia parameter
K_L, K_{L1}, K_D, K_{D1}	= empirical constants
l	= ice height, m
l_{int}	= ice adhesion width (interior ice thickness), m
M	= freestream Mach number
r/c	= airfoil leading-edge radius-to-chord ratio
t	= ice thickness, m
t/c	= airfoil thickness-to-chord ratio
T_c	= corrected temperature, °C
T_{GL}	= glaze ice boundary static temperature (T_{glaze}), °C
T_{ON}	= onset of ice static temperature, °C
T_R	= rime ice boundary static temperature, °C
T_s	= static temperature, °C
V	= local velocity, m/s (ft/s)
V_{helo}	= helicopter forward flight speed, km/h (knots)
W	= liquid water content, g/m^3
α	= airfoil angle of attack, deg
γ	= ratio of specific heats
Δ	= incremental quantity
ρ_I	= ice density, kg/m
τ	= icing time, s
τ_c	= corrected icing time, s

Introduction

THE potentially hazardous effects of ice accretion on the aerodynamic surfaces of aircraft have long been recognized. NACA and the fixed-wing industry initiated efforts to understand and counter the aircraft icing problem in the 1920s and increased the level of research activity during the 1940s and 1950s. These efforts concentrated on airfoil sections applicable to fixed-wing aircraft and the lower-speed range associated with most fixed-wing icing encounters. Renewed interest in icing research, including rotorcraft icing research, began in the late 1970s. However, the existing data base on ice accretion and its effects has been insufficient to fully understand and predict the rotor ice accretion phenomenon. To expand the data base, NASA supported the artificial ice testing of 10 two-dimensional models in the National Research Council of Canada (NRC) High-Speed Icing Wind Tunnel to Mach numbers up to 0.7 and several simulated ice configurations in both the NRC tunnel and the Ohio State University (OSU) Transonic Airfoil Facility. The objectives of this test included the acquisition of two-dimensional rotorcraft airfoil icing and simulated ice performance data representative of the helicopter operating environment and the development of empirical ice accretion and incremental lift, drag, and pitching moment relationships.

The high-speed ice accretion program is reported in Refs. 1-3.

Test Apparatus and Test Procedure

The NRC High-Speed Icing Wind Tunnel is a closed-circuit refrigerated wind tunnel. The test section is 12 in. square by 18 in. long. The high-speed test section has a maximum Mach number of 0.77 with an airfoil model installed. Oscillatory angle, to simulate the inflight variation of a helicopter blade angle, was provided by a pneumatic actuator at frequencies up to 10 Hz and amplitudes up to ±4.5 deg around the semichord point on the airfoil. The OSU 6×22 airfoil wind tunnel[4] was used during the cast ice phase of the test program.

A total of 10 airfoil models were used during these tests. The dimensional characteristics of these models are shown in Table 1. The NACA 0012 model was molded from an aluminum/epoxy mixture, the VR-7 model was machined steel, the OH-58 tail rotor blade (NACA 0012 airfoil) was a flightworthy aluminum blade, and the NACA 0011.5 model was a section of an aluminum model rotor blade. The remain-

Presented as Paper 85-0337 at the AIAA 23rd Aerospace Sciences Meeting, Reno, NV, Jan. 14-17, 1985; received March 22, 1985; revision received April 30, 1986.

*Senior Engineer, Aerodynamics, Sikorsky Aircraft Division. Member AIAA.

†Aerodynamicist, Sikorsky Aircraft Division.

ing five models were machined from stainless steel. The SC1095 airfoil was modified by the addition of an epoxy/fiberglass leading-edge piece to form the SC1094 R8 model. The models were selected to provide a range of rotorcraft airfoil contours (see Fig. 1). The NACA 0012 represents the first generation of helicopter airfoils and the VR-7 and the SC1095 family represent airfoils in use on current production helicopters. The SSC-A09 and circulation control models are advanced airfoils.

Baseline dry air data were obtained prior to ice accretion. Ice was accreted with the airfoil either stationary or oscillating at constant values of liquid-water concent (LWC), droplet size, and total temperature for a specified time. Following an icing encounter, steady-state data records consisting of tunnel parameters and airfoil pressures were taken. Planform and end view photographs were taken and the ice was cut to allow a tracing of the ice shape onto a template. The ice was also measured to provide more quantitative information on the geometry of the ice formation. Runs to define the effects of temperature, droplet size, and icing time were made for selected cases.

The OSU simulated ice test phase of the test program involved the acquisition of aerodynamic data for a limited matrix of Mach number/angle-of-attack conditions for the clean airfoil and cast ice shape.

Ice Shapes

The type of ice on an airfoil is governed by the rate that the supercooled water droplets freeze on the airfoil surface. The ice shapes fall into two main categories: dry growth (rime) and wet growth (glaze). The wet growth category can be broken further into three subcategories: beak, double-horned, and rounded glaze ice. Rime and glaze ice have traditionally been defined by their shape, but a review of the icing processes and the data from this test show that glaze ice can indeed have a streamlined shape, especially when the airfoil has been oscillating. For dry growth, the droplets freeze on contact with the airfoil surface and air is trapped in the ice, causing an opaque appearance. Wet growth ice, where the water runs back along the airfoil or along existing ice, is clearer in appearance. Ice that has the attributes of both rime and glaze ice has been referred to as glime by some experimenters and mixed icing by others. Beak ice forms on the airfoil in the region of high negative static pressure at moderate-to-high angles of attack. These ice types are illustrated in Fig. 2. Oscillation extends the chordwise ice coverage and decreases the depth of the depression between the horns of double-horned ice.

The NRC icing test data have been used to relate ice thickness to the ice height and to the adhesion width at the airfoil surface for glaze ice. Figure 3 shows ice dimension data for the NACA 0012 airfoil. The ice adhesion width is a function of liquid-water content, icing time (ice thickness), and airfoil shape (Fig. 4).

The boundary between ice types and for the onset of icing was determined experimentally during this test. The onset boundary was determined by slowly reducing tunnel temperature with the spray on. The first ice formed in the region of peak suction on the airfoil and was of the beak type.

Table 1 Dimensions of test models

Airfoil	t/c	Chord, cm (in.)
NACA 0012	0.120	15.24 (6.00)
SC1095	0.095	15.24 (6.00)
SC1094 R8	0.094	15.39 (6.06)
SC1012 R8	0.120	15.39 (6.06)
SSC-A09	0.090	15.24 (6.00)
VR-7	0.120	16.21 (6.38)
OH-58 tail rotor blade	0.120	13.34 (5.25)
NACA 0011.5	0.115	6.83 (2.69)
Circulation control	0.213	15.24 (6.00)

Beak ice (see Fig. 5) forms because of the reduced kinetic heating and enhanced evaporation in the suction region. The onset of icing temperature is

$$T_C = 0 = \left[(T_s + 273.15) \times \left(1 + \frac{\gamma - 1}{2} r M^2 \right) + 0.33(\alpha - 6) \right] - 273.15 \quad (1)$$

where r is a boundary-layer recovery factor represented by

$$r = 0.0944MW^2 + 0.385MW + 0.98M^3 - 1.33M - 0.0283W^2 - 0.115W + 1.077 \quad (2)$$

Figure 6 shows the hover correlation of observed and predicted ice extents for the UH-1H aircraft.[5,6]

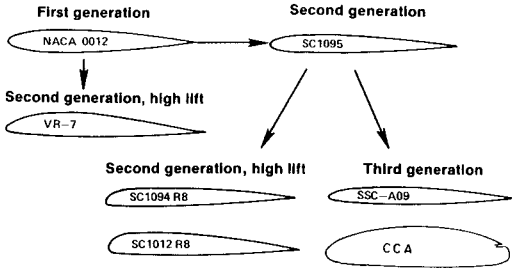

Fig. 1 Airfoil contours.

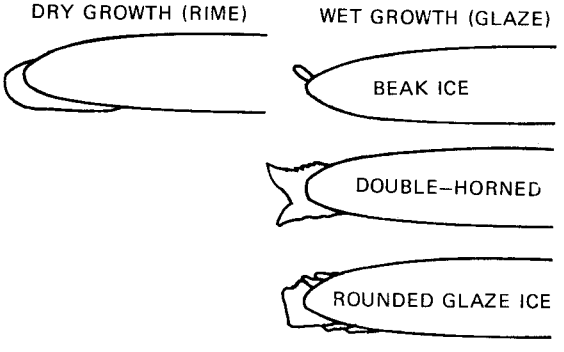

Fig. 2 Ice shape types.

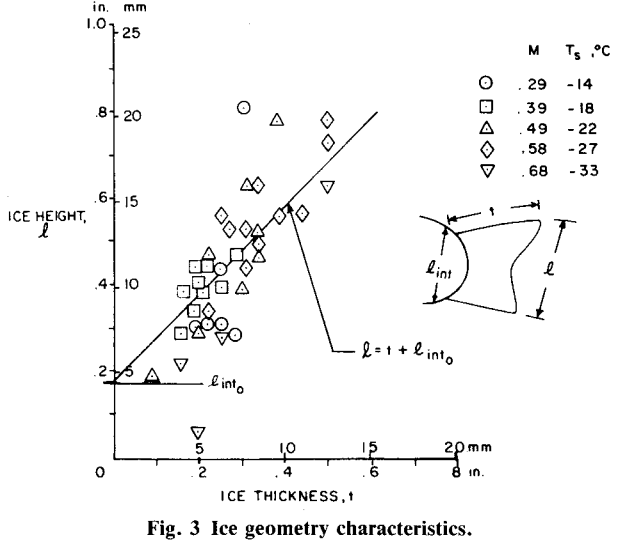

Fig. 3 Ice geometry characteristics.

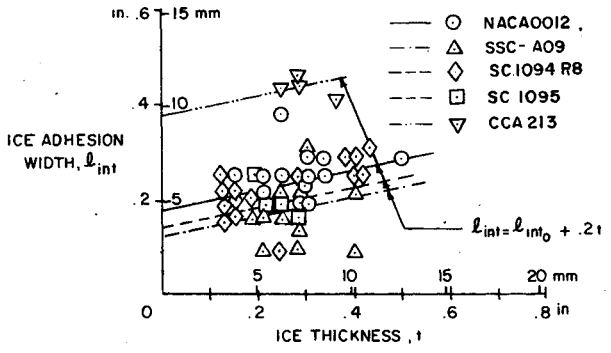

Fig. 4 Ice adhesion width vs ice thickness.

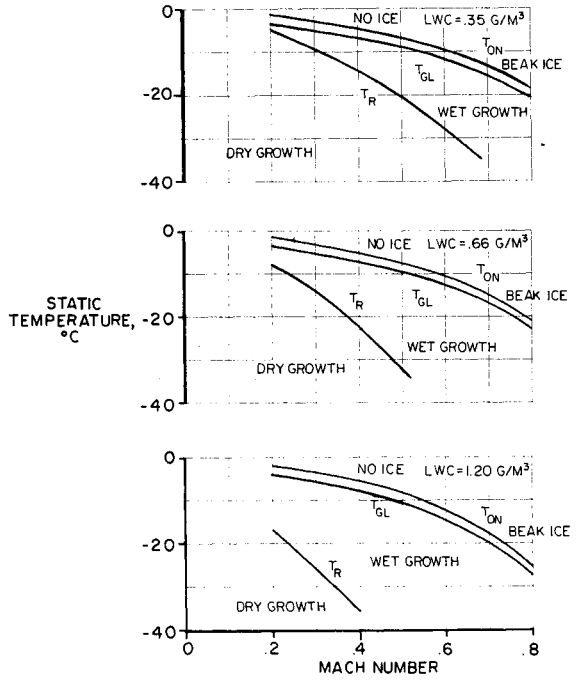

Fig. 5 Ice type boundaries, angle of attack = 6 deg.

Figure 7 illustrates the lift increment at a constant angle of attack and the drag and moment increments at a constant lift coefficient (the lift coefficient of the iced airfoil) that result from ice accretion for increasing exposure times. For a constant Mach number and angle of attack, approximately linear relationships are observed for airfoil performance degradation as LWC increases.[1] Ice thickness increases nonlinearly. With the Mach number and LWC constant, the airfoil performance degradation is nonlinear with increasing angle of attack. The lift and pitching moment increments for the thicker (12%) airfoils were smaller than those for the 9–9.5% thick airfoils. The drag penalties tended to be greater for the thick airfoils. Mach number had little effect on the drag increments for the thinner airfoils, but did have an impact on the NACA 0012 and VR-7 airfoils. Mach number had a greater impact on lift increments for the more cambered airfoils.

Selected icing conditions were repeated for the airfoil oscillating sinusoidally at a frequency of 5 Hz (typical 1/rev rotor frequency) with an amplitude of 9 deg. The effect of oscillation on lift and pitching moment are small, but the drag was reduced when compared to ice accreted without oscillation (Fig. 8). The angle of attack was changed from the ice accretion angle for several test conditions. The data show that the force and moment increments are dependent on the data

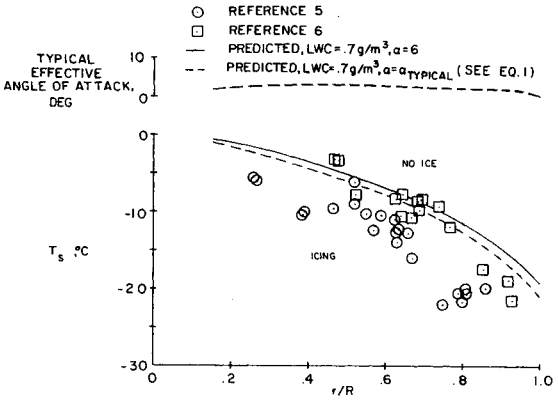

Fig. 6 Icing extent correlation for UH-1H helicopter.

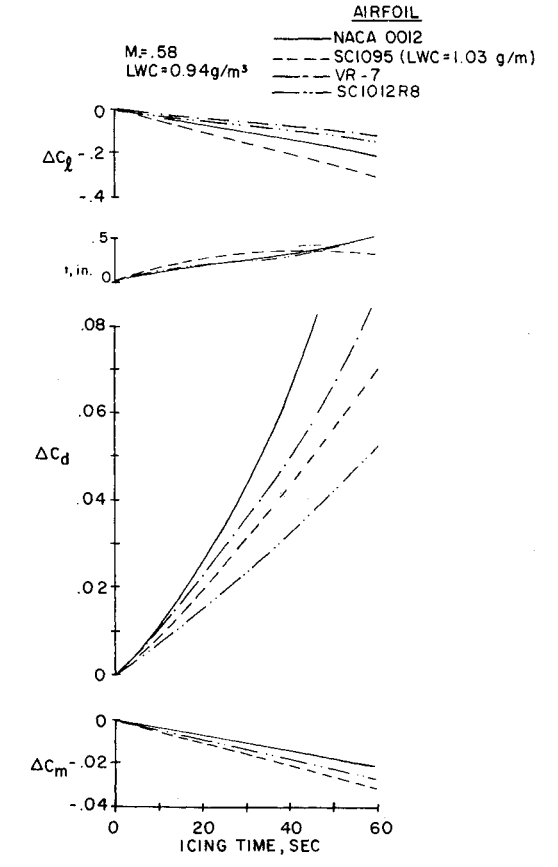

Fig. 7 Effect of icing time at an angle of attack of 6 deg.

acquisition angle, rather than the ice accretion angle, at angles up to about 6 deg. At higher angles, the lift and drag increments are larger than expected from ice accretion data. The icing lift and drag increments are higher at temperatures within 8–10°C of the onset temperature than they are at colder temperatures (see Fig. 9). The surface of the ice is rougher and the ice horns form further aft on the airfoil at warmer temperatures.

Icing Relationships

The two-dimensional NRC wind tunnel data has been used to develop relationships for ice thickness and lift, drag, and pitching moment increments, which give improved prediction capability beyond that found in Refs. 7 and 8. These relationships include terms shown to be important by the results of these tests and prior icing research: icing time, modified inertia parameter, liquid-water content, temperature, airfoil thickness ratio, angle of attack, and airfoil leading-edge radius

of curvature. As the airfoil enters drag divergence or stall, the aerodynamic increments are very nonlinear. The equations given below do not include terms to produce good results for those conditions.

The lift increment appears to be primarily a function of the modified inertia parameter, liquid water content, icing time, angle of attack, airfoil chord, airfoil thickness, and temperature. Using these terms, empirical constants were determined to fit the test data base, resulting in the following relationship:

$$\Delta C_l = -0.01335K_0(t/c)\,[\alpha+2 + K_{L1}0.00555(\alpha-6)^2]K_L \times 0.1524(W\tau_c/c) \quad (3)$$

where K_L and K_{L1} are functions of temperature and angle of attack as shown in Fig. 10 and τ_c is a corrected icing time. The corrected time was established from rotorcraft data that show that the torque rise does not increase linearly with time. There appears to be a maximum torque rise for a given rotor system for specified icing conditions due to shedding and accretion of ice reaching a state of equilibrium (see Fig. 11, for example). An effective or corrected icing time is produced by modifying the actual exposure time as shown in Fig. 12. Similitude (chord) terms are based on Ref. 9. Figure 13 shows the correlation of this relationship with NRC NACA 0012 icing data, where ΔC_l error is the measured ΔC_l – predicted ΔC_l.

Incremental rime ice drag is represented by a relationship that is similar in form to that of Ref. 7, but with the equation constants reduced and terms included to account for the observed effects of angle of attack and airfoil oscillation,

$$\Delta C_d = \left(0.158\ell n\frac{k}{c} + 175\frac{V}{\rho_I c}EW\tau_c + 1.70\right)\left(\frac{\alpha+6}{10}\right) \times \left(1-8\Delta C_d'\frac{V_{\text{helo}}}{278}\right) \times C_{d_{\text{no ice}}} \quad (4)$$

where $\Delta C_d'$ is the ΔC_d for $V_{\text{helo}}=0$ and $C_{d_{\text{no ice}}}$ is the clean airfoil drag [if $C_{d_{\text{no ice}}}$ is >0.0210, use 0.0210 in Eq. (4)].

The rime ice drag increment is primarily Reynolds number dependent and the effect of chord is included in the skin friction and accumulation parameter ($VW\tau_c/\rho_I c$) terms of Eq. (4). For glaze and beak ice, the drag coefficient increment varies according to the variables of Eq. (3), as well as the airfoil leading-edge radius and Mach number. The constants of the glaze and beak ice drag equation have been determined empirically from tunnel data. The resulting glaze and beak ice drag increment is represented by

$$\Delta C_d = \left[K_{D1} \times 0.00686K_0\left(\frac{t}{c}\right)^{1.5}(\alpha+6) - 0.0313\left(\frac{r}{c}\right)^2 + K_D 0.006M^{2.4}\right] \times 0.1524\frac{W\tau_c}{c} \times \left(1-8\Delta C_d'\frac{V_{\text{helo}}}{278}\right) \quad (5)$$

where K_D and K_{D1} are functions of temperature as shown in Fig. 10.

Figure 14 shows the degree of correlation of these equations with the NRC NACA 0012 test data. While the other airfoils correlate well, the equations tend to underpredict the drag at high ΔC_d levels for the NACA 0012 airfoil. The reason for this difference is not known.

Incremental pitching moment is represented by an empirically derived relationship applicable over the full range of tested ice types, using the variables of Eq. (5). This relationship is

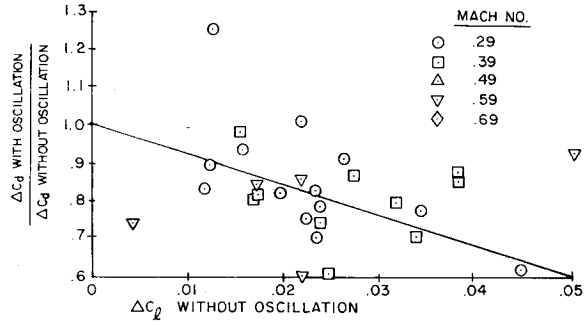

Fig. 8 Effect of airfoil oscillation on the drag coefficient.

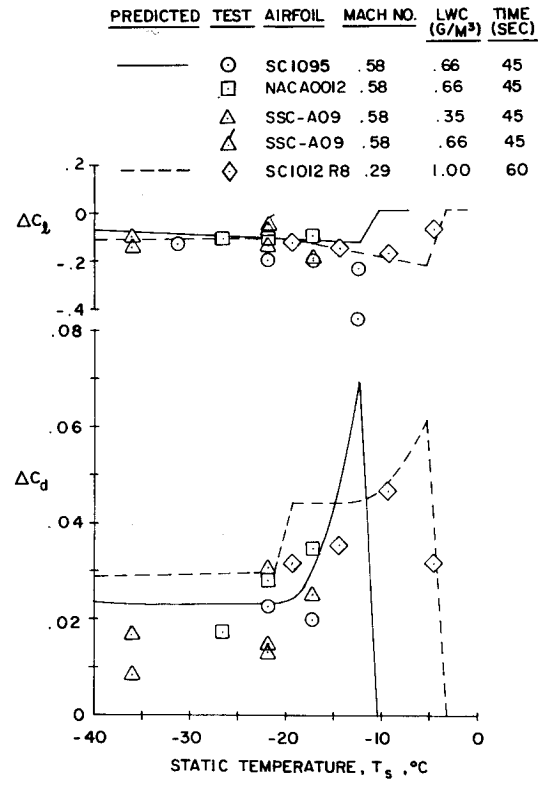

Fig. 9 Effect of static temperature on the drag coefficient.

$$\Delta C_m = \left[\frac{(0.00179-0.0045M)\,0.000544K_0\alpha}{(t/c)^{2.7}} + 0.00383M\left(1-63.29\frac{r}{c}\right)\right] \times 0.1524\frac{W\tau_c}{c} \quad (6)$$

The correlation of this relationship with NRC data is given in Ref. 1.

Ice thickness and shedding characteristics are difficult to predict and considerable empiricism is required. The model adapted in this study is a function of the rime and onset of ice boundaries and the amount of water that strikes the airfoil. A complete development of accretion rate and ice thickness relationships are given in Ref 1.

Comparison with Bragg and Gray Correlations

The correlations developed from the NRC wind tunnel data have been compared to the relationships developed by Bragg[7] and Gray.[8] Bragg's rime ice fit gives higher drag coefficient increments than indicated by the NRC test data (see Fig. 15). The correlations of Gray were developed from limited data

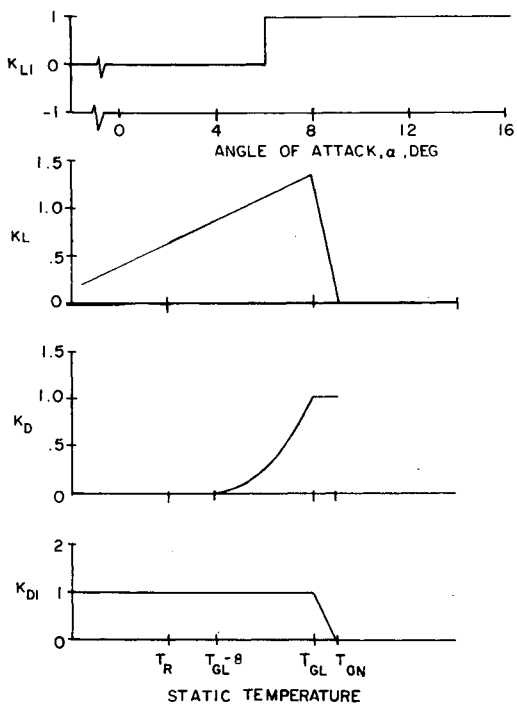

Fig. 10 Temperature and angle-of-attack factors.

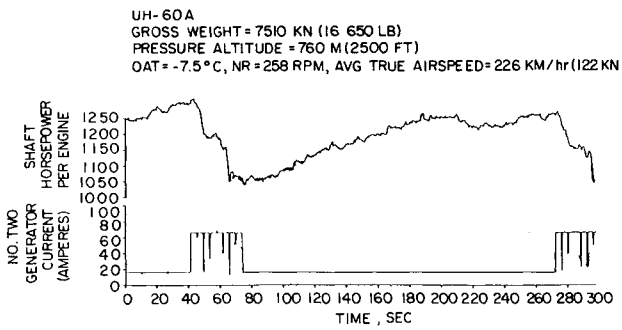

Fig. 11 Rotor torque rise trend vs icing time.

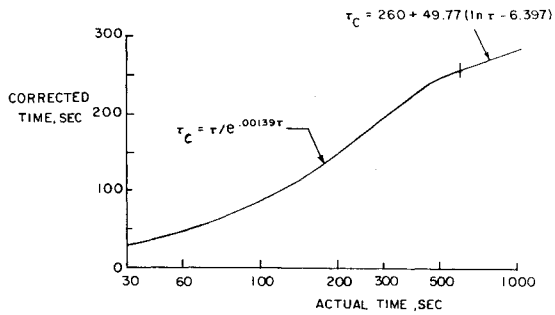

Fig. 12 Corrected icing time vs actual exposure time.

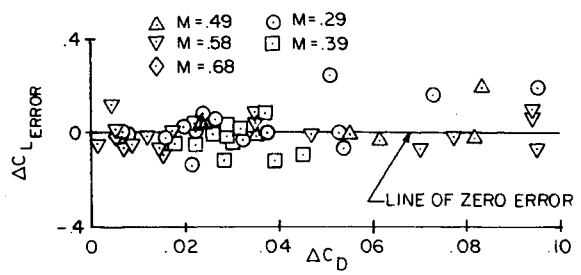

Fig. 13 Correlation of incremental lift relationship with NRC data for the NACA 0012 airfoil.

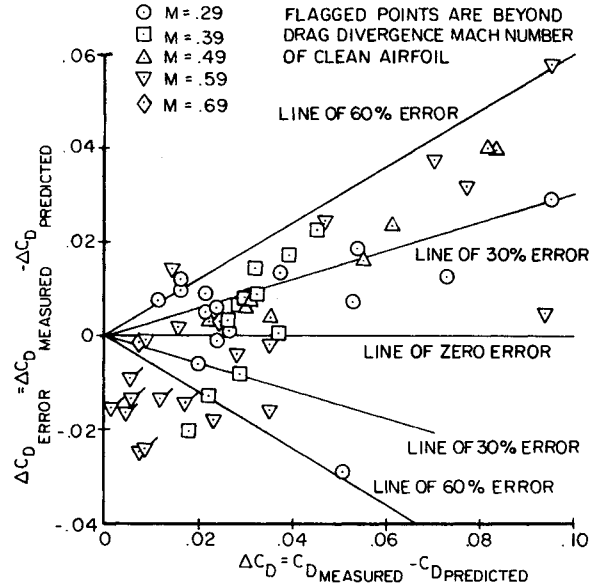

Fig. 14 Correlation of incremental drag relationship with NRC data.

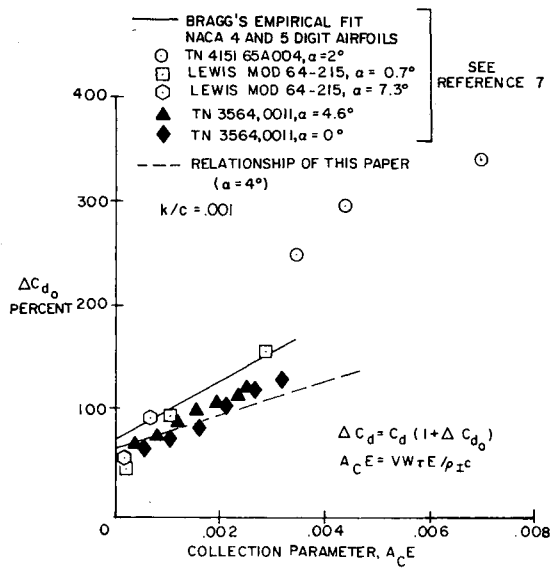

Fig. 15 Rime ice drag coefficient correlation.

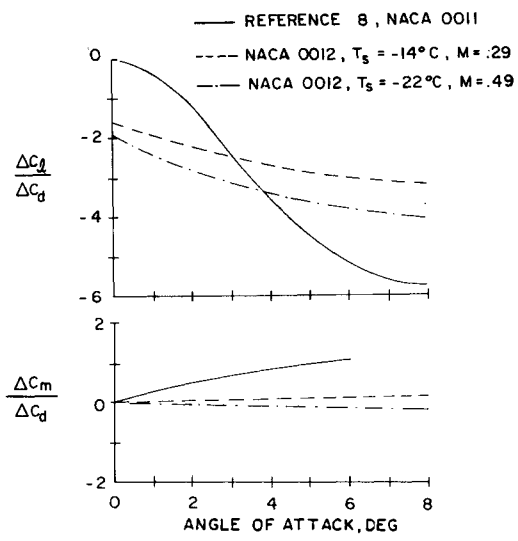

Fig. 16 Gray lift and pitching moment coefficient vs NRC data.

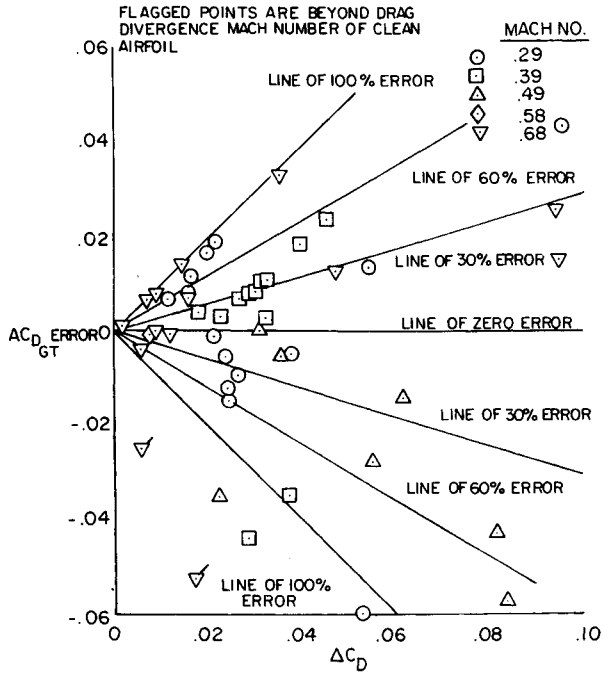

Fig. 17 Gray drag coefficient correlation error vs NRC data for the NACA 0012 airfoil.

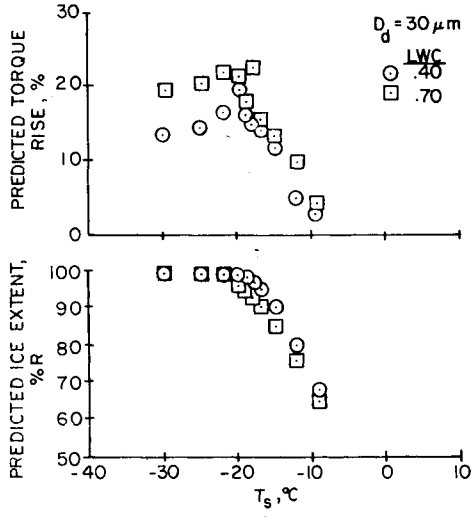

Fig. 18 Predicted torque rise and ice extent vs static temperature, UH-1H in hover.

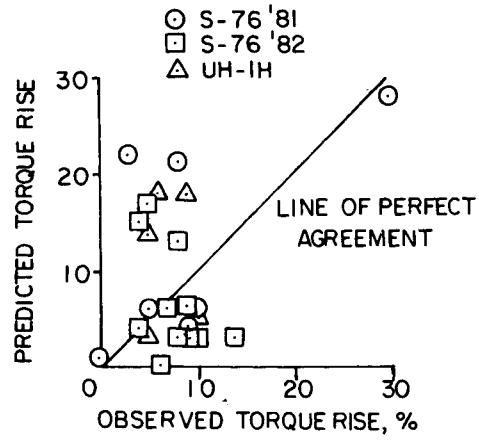

Fig. 19 Rotorcraft torque rise correlation in hover.

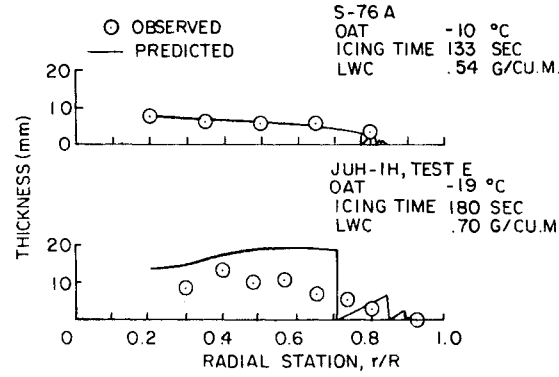

Fig. 20 Rotorcraft ice thickness correlation.

and do not contain terms to account for the variables found important during the analysis of the NRC test data. The lift increment correlation developed herein does not follow the $\Delta C_l/\Delta C_d$ form of Ref. 8. A similar comparison has been made with the pitching movement curve presented in Ref. 8 (see Fig. 16). The current work shows a significant Mach number effect on pitching moment that was not observed during prior tests.

Many researchers have recognized the shortcomings of the drag correlation of Gray. While correlating well with the data base available to Gray in 1957, significant scatter on both the high and low side of the correlation exists when compared with recent NASA data[7] and the recent NRC data presented herein. In addition to accuracy problems using the Grey correlation, the portion of the high Mach number data where the total temperature exceeds 0°C (32°F) must be discarded, since the Gray relationship cannot be solved for those high total temperatures. Figure 17 shows the error for the Gray correlation versus the measured drag coefficient increment for the NACA 0012 airfoil.

Correlation with Rotorcraft Data

The two-dimensional icing relationships have been programmed and adapted for use in hover and level flight codes. The existence and type of ice is based on the average blade segment velocity and angle of attack, while the lift and drag increments are based on local conditions. The rotorcraft icing code has been used to compute hover torque rise for S-76A and JUH-1H hover artificial icing data. The key to the success of a prediction method is the determination of ice extent and the type of ice that forms on the blade. Figure 6 shows that the method developed herein predicts the onset of ice and, therefore, the ice extent well. The importance in determining the onset of icing and providing an accurate measure of temperature is illustrated by the sensitivity of the power/temperature relationship given in Fig. 18. For the warmer ice conditions ($T_s > -20°C$), the predicted UH-1H torque rise increases by nearly 2% for each 1°C reduction in temperature and the ice extent increases 4% for each 1°C reduction in temperature. The correlation of predicted and measured torque rise for hover conditions is shown in Fig. 19. Much of the scatter can be attributed to variability within the flight test data set. However, part of the deviation contained in Fig. 19 appears to be temperature related. The observed torque rise exceeds the predicted torque rise for warmer temperatures, underpredicting the ice extent. The observed torque rise is less than the predicted torque rise for colder temperatures and the prediction method appears to overpredict ice extent. Photographic data have been used to produce the shape data of Fig. 20, which shows that the predicted ice thicknesses agree well with S-76A observed thicknesses, but overpredicts the ice thicknesses measured on the JUH-1H helicopter. Shedding is predicted for each of these test conditions.

Conclusions and Recommendations

Testing in the NRC High-Speed Icing Wind Tunnel and the OSU Transonic Airfoil Facility has expanded the data base on iced airfoil performance. Systematic variations of environmental and tunnel conditions has yielded trends for the impact of these parameters. The influence of airfoil shape on icing was observed among the 10 airfoils tested. Molds of several ice shapes were used to fabricate ice castings for testing in the OSU and NRC wind tunnels.

Generally, lift and drag increments vary linearly with liquid-water content. Increasing Mach number has a greater impact on the 12% thick airfoils than for the 9% thick airfoils. The data have been generalized into a series of equations, providing a prediction of ice thickness and force and moment coefficients with an accuracy of about 30%. The relationships have been incorporated into rotorcraft performance codes to give ice extent and torque rise information. An assessment of the accuracy of the torque prediction method is difficult because of the observed scatter in the helicopter performance flight test data.

Research in the field of rotorcraft icing is currently progressing more rapidly than during any other time period. It is apparent, however, that data to provide correlation information, especially rotor icing data, are lacking in detail and completeness. Recent NASA/Army flight research is providing quality data and the procedures adopted for that research should be extended to qualification test programs. The methodology presented in this report should be compared with rotor data and airfoil data taken in other icing and simulated ice tests to substantiate and improve the prediction accuracy.

References

[1]Flemming, R.J. and Lednicer, D.A., "High Speed Ice Accretion On Rotorcraft Airfoils," NASA CR 3910, Aug. 1985.

[2]Flemming, R.J. and Lednicer, D.A., "Experimental Investigation of Ice Accretion on Rotorcraft Airfoils at High Speeds," AIAA Paper 84-0183, Jan. 1984.

[3]Flemming, R.J., Shaw, R.J., and Lee, J.D., "The Characteristics of Simulated Ice On Rotorcraft Airfoils," AHS Paper A-85-41-66-J000, May 1985.

[4]Lee, J.D., Gregorek, G.M., and Korkan, K.D., "Testing Techniques and Interference Evaluation In the OSU Transonic Airfoil Facility," AIAA Paper 78-1118, July 1978.

[5]Wilson, G.W., "Helicopter Icing—Testing and Certification," *Journal of the American Helicopter Society,* Vol. 27, No. 2, April 1982.

[6]Abbott, W.Y. et al., "Evaluation of UH-1H Hover Performance Degradation Caused by Rotor Icing," USAAEFA Project 82-12 Final Report, Aug. 1983.

[7]Bragg, M.B., "Rime Ice Accretion and Its Effect On Airfoil Performance," NASA CR 165599, March 1982.

[8]Gray, V.H., "Prediction of Aerodynamic Penalties Caused by Ice Formations On Various Airfoils," NASA TN D-2166, Feb. 1964.

[9]"Aircraft Icing," AGARD Advisory Rept. 127, Nov. 1978.